Optogenetic control of YAP can enhance the rate of wound healing

P. J. Y. Toh[1§], M. Sudol[1,2] and T. E. Saunders[1,3,4*]

[1] Mechanobiology Institute, National University of Singapore, Singapore

[2] Icahn School of Medicine at Mount Sinai, New York City, USA

[3] Institute of Molecular and Cell Biology, A*STAR, Singapore

[4] Warwick Medical School, University of Warwick, United Kingdom

§ Current address: Novo Nordisk Foundation Center for Basic Metabolic Research, Faculty of Health and Medical Sciences, University of Copenhagen, Denmark

* For correspondence: T.E.S. (timothy.saunders@warwick.ac.uk)

Abstract

Tissues need to regenerate to restore function after injury. Yet, this regenerative capacity varies significantly between organs and between species. For example, in the case of the heart, while some species retain full regenerative capacity throughout their lifespan, human cardiac cells display only limited ability to repair injury. Here, we investigate in cell culture the role of the YAP, a transcriptional co-regulator with a pivotal role in growth, in driving repair after injury. Utilising an optogenetic version of YAP that enables precise control of pathway activation, we show that YAP can increase the speed of wound healing in H9c2 cardiomyoblasts. Interestingly, this is not driven by an increase in proliferation, but by collective cell migration. We subsequently dissect specific phosphorylation sites in YAP to identify the molecular driver of accelerated healing. Overall, our results reveal that YAP activation – through controlled optogenetic activation - can potentially enhance wound healing in a range of conditions.

Keywords: Hippo-YAP, optogenetics, wound healing

Introduction

During myocardial infarction, blood flow to the heart is severely limited or completely cut off by plaque or cholesterol blockages. Without oxygen and nutrients, heart muscles surrounding the region of the blocked vessel begin to necrose. Acute myocardial injury can kill 25% of cardiomyocytes, rendering them non-functional.(1) Pharmacological management after a heart attack only serves to prevent another episode from occurring and there are no known strategies to restore the full capacity of the heart. This in part due to the human heart having a very limited ability to regenerate post injury.(2) This lack of regenerative capability is in contrast to other organs, such as the liver or gut.(3) Further, other organisms show a greater capacity to regenerate injured heart tissue post-embryonic development: young mice (<7 days) can repair heart wounding; and in zebrafish the potential to regenerate heart tissue remains throughout the lifespan.(4,5) Therefore there is a demand to find strategies to induce cardiac regeneration in humans. Though new cardiomyocytes can be synthesised *ex vivo* from embryonic stem cells and organise to form contractile tissues, injected cells have an embryonic lineage and can generate arrythmias.(6,7) Recipients also need to be immunosuppressed for transfusion, which itself is a complex procedure. Alternative strategies to induce human heart tissue repair and regeneration are still heavily sought after.

A strategy to circumvent the above complexity is to stimulate the endogenous proliferation potential of cells in repair. The key idea is to effectively mimic developmental processes, reviving pathways that are switched off postnatally. This approach has seen positive results in transgenic mice models, where activated YAP promotes cardiac regeneration by inducing reparative genetic programs to re-enter the cell cycle and activate proliferative genes in cardiomyocytes.(8–10) The Hippo-YAP pathway is highly implicated in development and

52 regenerative processes, due to its role in driving cell proliferation, migration and
53 mechanosensing.(11,12) The pathway is constructed principally from a kinase cascade that
54 culminates at the transcriptional co-activator YAP and its paralogue TAZ. Phosphorylated
55 YAP/TAZ triggers its cytoplasmic sequestration(13,14) or degradation,(15) while
56 unphosphorylated YAP/TAZ can translocate into the nucleus and bind to transcription factors
57 TEAD1-4.(16–18) This stimulates the expression of a range of genes that typically lead to pro-
58 survival outcomes in the cell.(19–21) The nucleocytoplasmic distribution of YAP/TAZ is a
59 key determinant of its activity. Therefore, manipulating the YAP/TAZ localisation can provide
60 a tool to control the subcellular activation of the Hippo-YAP pathway.
61
62 Previous studies have shown that the MAPK/ERK pathway is a key regulator of organ
63 regeneration(22,23), and crosstalk with the Hippo-YAP pathway in cardiomyocytes reactivates
64 cell proliferation.(24,25) ERBB2 (a member of the EGFR family) signalling induces a
65 phosphorylation mark on two non-canonical serine residues on YAP by ERK.(25) The
66 activating phosphorylation marks on S251 and S333 oppose the conventional deactivating
67 phosphorylation caused by LATS on S127. The phosphorylation mark at S127 generates a 14-
68 3-3 binding site, causing the cytoplasmic sequestration of phosphorylated YAP, accelerating
69 the nuclear export of YAP and inhibiting its co-transcriptional function inside the
70 nucleus.(26,27) Mutation of serine 127 to alanine has been reported to increase the activity of
71 YAP by preventing LATS phosphorylation.(28–30) Besides the phosphorylation site at S127,
72 another protein domain that regulates the localisation of YAP is the C-terminal PDZ-binding
73 motif,(31) a short motif of only five amino acid residues, -FLTWL at the very carboxyl terminal
74 end. The PDZ-binding motif allows YAP to bind to proteins containing the PDZ domain such
75 as ZO-2 and a deletion of this motif impairs the nuclear shuttling of YAP through ZO-2.(31)
76 However, similar to the S127A mutant, truncation of the PDZ-binding motif does not impair

77 the induction of TEAD-mediated transcriptional activity, only affecting its subcellular
78 localisation.(30,32) The YAP paralogue TAZ also contains a C-terminal PDZ-binding motif,
79 which has been shown to be required for its nuclear localisation.(14) Therefore, the PDZ-
80 binding motif appears to be a conserved sequence that is integral to the function of YAP/TAZ
81 as transcriptional co-regulators. However, how these phosphorylation marks and domains alter
82 the dynamics of YAP signalling – and subsequently its efficacy in regeneration – remain
83 unknown.
84
85 During regeneration, there are two main mechanisms for repair: (1) migration of newly
86 proliferated cells into the injured area; and (2) cell proliferation within the regenerating zone.
87 YAP is involved in wound healing, by limiting cytoskeletal and focal adhesion maturation to
88 promote cell motility.(33) YAP increases migration and invasiveness in a number of cell lines,
89 often stimulating epithelial-to-mesenchymal transition (EMT).(34) On top of enhancing cell
90 cycle progression, YAP also promotes cytoskeletal remodelling, responding to the mechanical
91 change during scar tissue formation post myocardial infarction.(35) YAP has also been shown
92 to be activated in cardiac fibroblasts after ischemic injury.(36)
93
94 While YAP activity has been shown to regenerate the mice heart after injury, caution must be
95 taken as over-proliferation can cause occlusive vascular diseases.(37) Therefore, having
96 control over the spatiotemporal localisation of YAP is important. Optogenetics provides such
97 a method,(38,39) whereby light activation can control protein behaviour, and we have recently
98 applied this to YAP (optoYAP).(40) Can optogenetic YAP be used to control regeneration after
99 wounding or injury? optoYAP is potentially a powerful tool to circumvent regenerative
100 limitations whilst retaining specific spatiotemporal control over its activity. Building upon our
101 previously reported work,(40) we utilised a range of cell lines, including H9c2 rat

102 cardiomyoblasts, as *in vitro* models to study how activation of YAP can promote repair post-
103 injury.[41,42]
104
105 Here, we report that activated optoYAP accelerates wound healing in two different cell lines,
106 driving cell migration that is essential during regeneration. In particular, we show that H9c2
107 cardiomyoblasts are responsive to optoYAP activation, inducing nuclear accumulation after
108 light activation. Nuclear optoYAP increases expression of downstream proliferative YAP
109 target genes *CTGF* and *CYR61*, as well as *TGF-β*, a transforming growth factor involved in
110 stem cell regulation and differentiation. This suggests that optoYAP can potentially be
111 applicable in regenerative studies of tissues – including cardiac tissues – by promoting the
112 renewal and replication of cells post-injury.
113
114 The Hippo-YAP pathway crosstalks with ERBB2 signalling during cardiac regeneration,
115 where ERK induces two activating phosphorylations (S251 and S333) on YAP.(25) To further
116 understand the potential mechanism for YAP function in regeneration, we generated
117 phosphomimetic mutants at both serine residues and observed that they had an elevated amount
118 of nuclear localisation in the dark as compared to wildtype optoYAP. However, the mutants
119 could still respond to light activation. Building upon the changes in basal distribution of mutant
120 optoYAP, we mutated the canonical LATS phosphorylation serine residue 127 to alanine,
121 preventing its inactivating phosphorylation effect on YAP. We observed that optoYAP S127A
122 was strongly nuclear localised before light activation and the nuclear signal was amplified after
123 light activation. By removing the C-terminal PDZ-binding motif, another regulatory domain of
124 YAP, we arrested the intrinsic nuclear localisation of YAP by preventing it from binding to
125 nuclear importins. However, optogenetic activation was still able to promote nuclear
126 localisation of this mutant through the NLS present on the optogenetic backbone. Overall, our

127 results reveal that optogenetic approaches provide a strategy for specific control over YAP
128 nuclear localisation (and hence activity) in both wildtype YAP and its mutants, thereby making
129 it a potential tool for driving tissue regeneration.
130
131 **Results**
132
133 *optoYAP activity in H9c2 cells:* Using a previously reported optoYAP for optogenetic control
134 of YAP nuclear import and export,(40) we transfected H9c2 cells with optoYAP and
135 characterised the construct in the rat cardiomyoblasts. We subjected transfected cells to
136 pulsatile light activation with 488 nm laser power at 0.15 mW for 1 second at a 30 second
137 interval, for a total of 20 minutes. We observed nuclear localisation of the optogenetic construct
138 after the 20 min activation window (Fig. 1A). After leaving the cells in the dark for a further
139 20 minutes, optoYAP translocated out of the nucleus and returned to the basal state before light
140 activation (Fig. 1A). The nuclear/cytoplasmic ratio of optoYAP almost doubled after the 20
141 min activation (Fig. 1B). Throughout the activation and recovery cycle, we tracked and imaged
142 the cells over time to obtain the nuclear import and export dynamics (Fig. 1B). The activation
143 (τ_a) and recovery (τ_r) time constants were calculated to be 4.6 ± 0.6 minutes and 13.5 ± 1.6
144 minutes respectively (Methods). These values are comparable with those obtained by using the
145 HEK293T cell line described previously.(40)
146
147 *Elevated downstream gene expression levels after optoYAP activation:* Following the light-
148 dependent nuclear localisation of optoYAP, we examined the functionality of nuclear localised
149 optoYAP by measuring the changes in downstream gene expression levels. We quantified the
150 transcript levels of *CTGF*, *CYR61*, and *TGF-β* in H9c2 cells after 48 hours of pulsatile light
151 activation (Fig. 1C). *CTGF* and *CYR61* are canonical YAP target genes that provide a readout

152 for optoYAP activity in the nucleus.(18,29) Additionally, we looked at *TGF-β* transcript levels
153 as it ©s an inflammation-related growth factor and is frequently involved in the migration and
154 invasion of tumour cells.(41) YAP has also been shown to be a mediator of *TGF-β*
155 signalling(42,43) and the pathway has been implicated in cardiomyocyte proliferation and
156 migration.(44,45)
157
158 We observed that the expression levels of all three genes probed were significantly upregulated
159 in cells containing activated optoYAP as compared to wildtype (WT) H9c2 (Fig. 1C). However,
160 the transcript levels of *CTGF* and *TGF-β* in transfected cells kept in the dark were also
161 significantly increased in comparison to wildtype controls, though clearly less than when light
162 activated. This suggests that there might be small amounts of nuclear optoYAP even without
163 light activation. However, the upregulation of gene expression across the three genes is
164 significant when comparing cells kept in the light versus dark. This shows that the optoYAP
165 construct is functional when nuclear localised and can trigger expression of downstream target
166 genes.
167

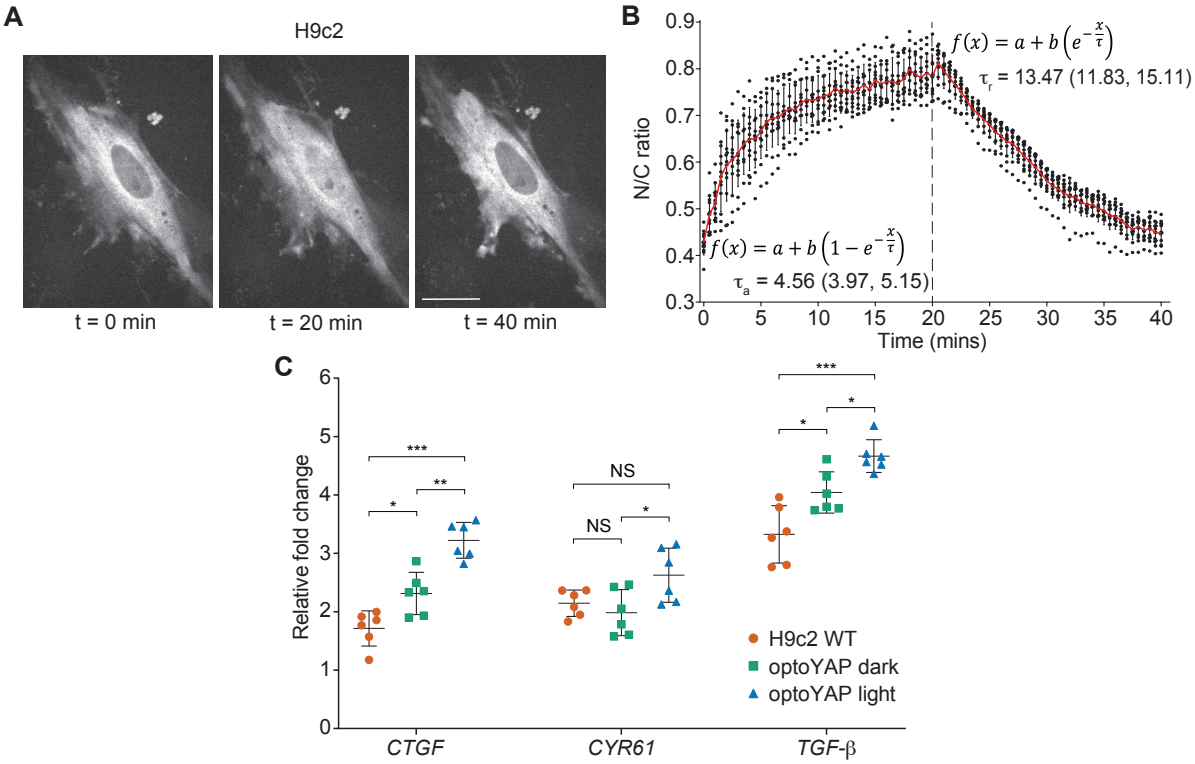

Figure 1. Characterisation of optoYAP in H9c2 cells. (A) Representative images of H9c2 cells transfected with optoYAP kept in the dark (t = 0 min), then subjected to pulsatile light activation for 20 min (t = 20 min), followed by recovery in the dark for a further 20 min (t = 40 min). Scale bar, 20 µm. **(B)** Quantification of activation (τ_a) and recovery (τ_r) time constant of optoYAP. Red line represents average nuclear/cytoplasmic ratio. Vertical dashed line represents time when 488 nm stimulation ceased. Numbers in brackets represent the 95% confidence interval of τ. n=12 cells. **(C)** RT-qPCR of YAP downstream genes. Cells were transfected with optoYAP, and transcript levels were assessed after 48 h of activation. Expression levels of *CTGF*, *CYR61*, and *TGF-β* were normalised to the housekeeping gene *EIF1B* and described as relative fold change. Horizontal bars represent mean and 95% confidence interval from 6 biological replicates from two independent experiments. NS: not significant, $*P < 0.05$, $**P < 10^{-2}$, $***P < 10^{-3}$.

183 *optoYAP promotes collective cell migration:* We next investigated the role of optoYAP during
184 wound healing, comparing endogenous and optogenetic YAP. Serum-starved cells were seeded
185 in wells 500 μm apart in serum-free media and the“"wound” size was quantified every 30
186 minutes until complete closure. We observed that optoYAP transfected H9c2 cells kept under
187 pulsatile light activation migrated faster over the wound as compared to transfected cells kept
188 in the dark or untransfected H9c2 (Fig. 2A). Wild type H9c2 cells took an average of 66 hours
189 for complete wound closure, in comparison to 60 hours taken for transfected cells in the dark
190 (Fig. 2B). Light activated optoYAP accelerated wound healing, taking an average of 53 hours,
191 a 20% improvement on the wild type cells. Though optoYAP transfected H9c2 cells kept in
192 the dark took a shorter time as compared to wildtype cells, light activation of the optogenetic
193 construct clearly bolstered this behaviour. Extracting the curve slopes in Fig. 2B inset, we see
194 that the activated optoYAP cells have significantly increased rate of closure.
195
196 We observed some cell proliferation events during the timelapse, despite the serum starvation
197 before and during the experiment, seen as bright, rounded cell doublets in Fig. 2A. We counted
198 the number of proliferation events that occurred during wound healing and observed that all
199 three conditions had similar number of proliferation events (Fig. 2C). This shows that the
200 differences in the time taken for wound healing observed in Fig. 2B is largely due to cell
201 migration and not proliferation.

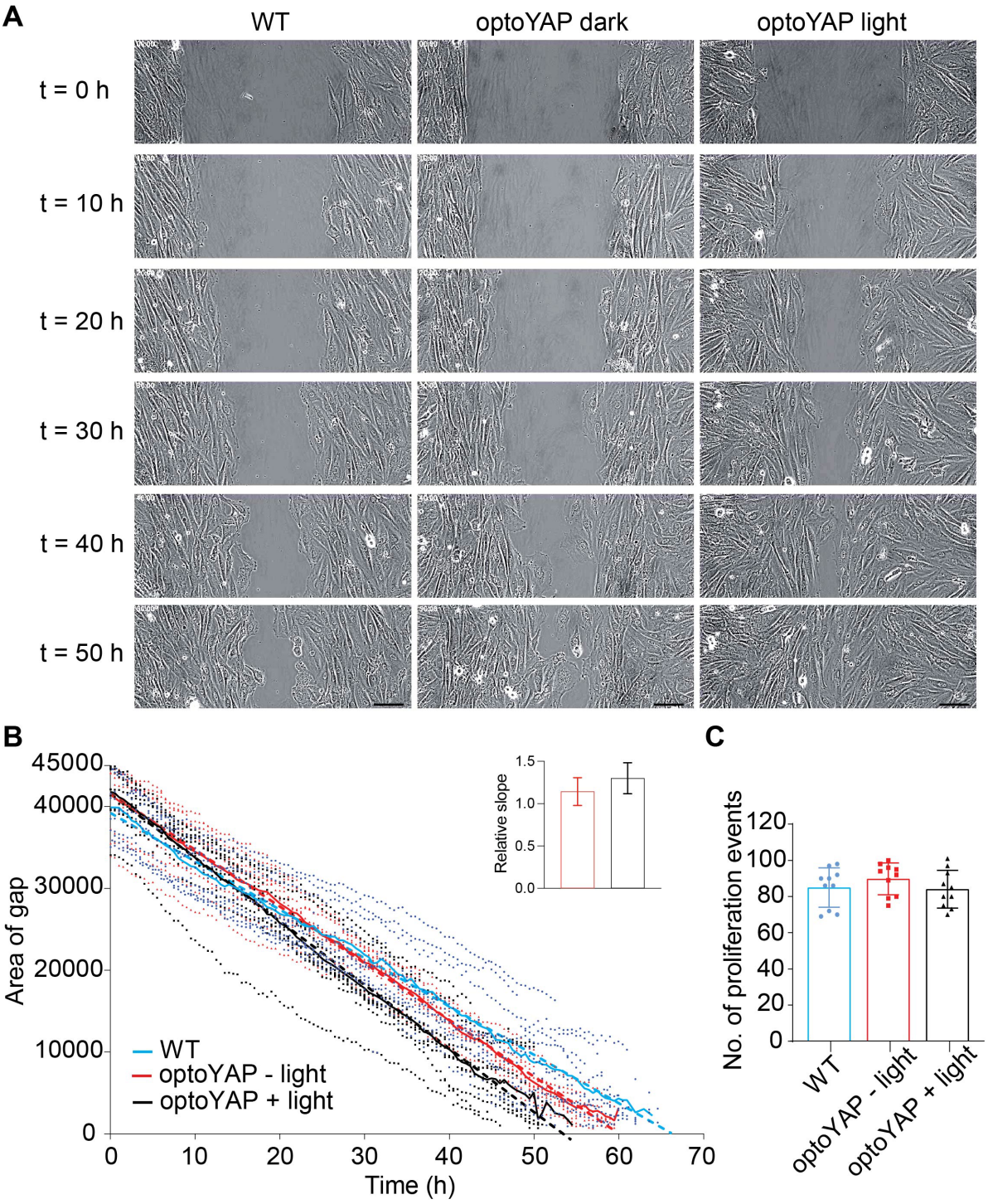

Figure 2. Wound healing assay in H9c2 cells. (A) Timelapse images of wildtype H9c2 cells or cells transfected with optoYAP under different light conditions, taken every 30 min until gap completely closes. Representative images shown at 10 h intervals. Scale bars, 100 µm. **(B)** Time taken for H9c2 cells for complete wound healing. Quantification of data in (A) over time. Bold lines represent mean and dashed lines represent linear regression fitted to the curve. n=10

208 from two independent experiments. Inset shows the measured slopes under different conditions
209 relative to wildtype (colours as in main plot), error bars are s.d.. **(C)** Number of proliferation
210 events counted during each wound healing experiment in (B). Bars represent mean and error
211 bars represents s.d..

212

213 We performed the same wound healing experiment in another cell line, MKN28, to exploit the
214 benefit of a CRISPR *YAP*$^{-/-}$ background previously reported.(46) This cell line enabled us to
215 precisely delineate the effect of optoYAP without any endogenous YAP present that might
216 confound the above results. Previous studies in the same cell line observed a difference
217 between wildtype and *YAP*$^{-/-}$ cells in a trans-well migration assay but not during wound healing
218 assays.(46) Therefore, we wanted to determine if our optoYAP construct changes the rate of
219 wound closure in these MKN28 *YAP*$^{-/-}$ cells.

220

221 As expected, the *YAP*$^{-/-}$ cells took much longer than the wild type or optoYAP transfected cells
222 for wound closure, taking 38 hours as compared to 33 hours for wild type MKN28 cells (Fig.
223 3A). This shows that endogenous YAP is required for cell motility during wound closure. In
224 MKN28 *YAP*$^{-/-}$ cells transfected with optoYAP, we noticed that those kept in the dark took a
225 faster time for wound closure (30.5 hours) in comparison to wild type cells. Light activated
226 optoYAP transfected *YAP*$^{-/-}$ cells had an accelerated rate of wound closure, taking only 29 hours
227 for the wound to close completely. This is supported by analysis of the slope of the curves (Fig.
228 3A inset). These results support the conclusion that endogenous YAP is involved in cell
229 migration and optoYAP further accelerates wound healing in MKN28 cells. Globally, it was
230 noteworthy that the MKN28 cells took a shorter time for wound closure (<40 hours) as
231 compared to the H9c2 cells (>50 hours).

232

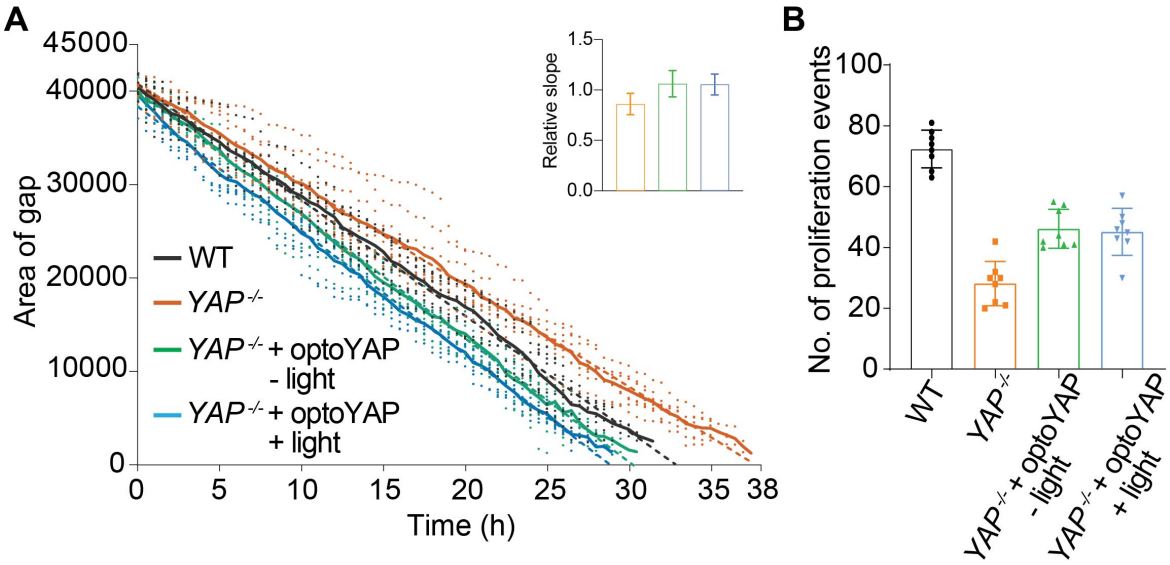

Figure 3. Wound healing assay in MKN28 variants. (A) Wildtype (WT) MKN28 and MKN28 *YAP*$^{-/-}$ cells transfected with optoYAP were seeded in culture wells 500 µm apart. The size of the gap was tracked every 30 min until it was completely closed. Bold lines represent mean and dashed line represents linear regression fitted to curve. n=8 from two independent experiments. Inset shows slope of lines relative to wildtype (colours as in main plot), with error bars representing s.d.. **(B)** Number of proliferation events in each experiment in (A). Bars represent mean and error bars represents s.d..

As with the H9c2 cells, we observed several proliferating MKN28 cells in the cell islands during wound closure. We counted the number of proliferation events and compared it amongst the MKN28 variants (Fig. 3B). Unsurprisingly, the *YAP*$^{-/-}$ variants had the least amount of proliferation events (28 ± 7), less than half of the wild type cells (72 ± 6) over the entire time course. Since YAP plays an important role in proliferation, knocking out YAP naturally reduces cell proliferation, which might explain the longer time taken for wound closure in *YAP*$^{-/-}$ cells as compared to wild type. Both optoYAP transfected *YAP*$^{-/-}$ cells under light (45 ± 7) or dark (46 ± 6) conditions had similar number of proliferation events, but still less than wild type cells. Despite less proliferation observed in optoYAP transfected *YAP*$^{-/-}$ cells, the time

251 taken for wound closure is shorter than wild type cells. This shows that optoYAP speeds up
252 the rate of wound closure in *YAP*$^{-/-}$ cells, seemingly by inducing cell migration. However, cell
253 proliferation plays a crucial part in wound closure, and it is important to understand the fine
254 interplay between proliferation and migration as revealed here by using CRISPR/Cas9-
255 generated *YAP*$^{-/-}$ MKN28 cells.(46)
256
257 *Changes in nuclear localisation of optoYAP phosphorylation mutants:* Above, we have shown
258 that YAP plays a role in wound healing, including in cardiomyocytes. Phosphorylation of YAP
259 on two ERK activating sites appears to be critical in this response,[26] but the dynamics remain
260 poorly understood. To explore this further, we synthesised three phosphomimetic optoYAP
261 mutants by substituting serine to aspartic acid on either S251 or S333, or both. We did this in
262 HEK293T cells due to their ease of transfection over H9c2 or MKN28 cells. We did not observe
263 distinct nuclear localisation differences amongst the three mutants (Fig. 4A). Comparing the
264 basal nuclear localisation of the three mutants, we observed that the double mutant had a
265 significantly higher initial nuclear localisation compared to the S251D mutant, but not the
266 S333D mutant (Fig. 4B). The mutants all displayed clear response to light activation (Fig. 4B-
267 D). They also displayed higher initial nuclear localisation over wildtype (Fig. 4E).

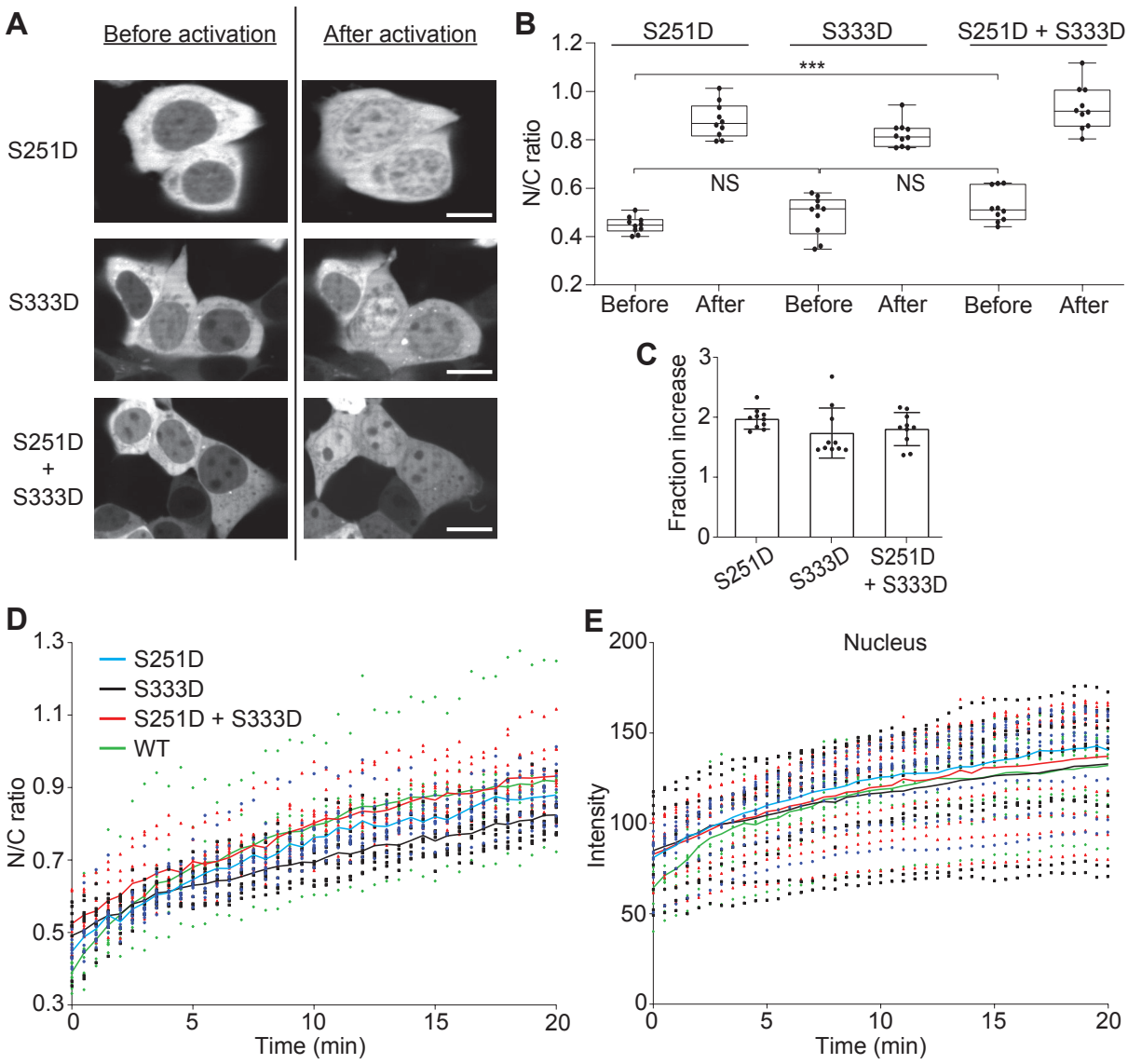

Figure 4. Point mutations of optoYAP at ERK phosphorylation serine residues. (A) Three mutants containing phosphomimetic of ERK target residues at S251, S333 or both S251 and S333. Representative images of HEK293T cells transfected with different mutant optoYAP before and after exposure to pulsatile light activation. Scale bars, 10 µm. **(B)** Quantification of cells from (A), measuring nuclear to cytoplasmic ratio of optoYAP before and after light activation for each mutant. NS: not significant, ***$P < 10^{-3}$. **(C)** Fraction increase of N/C ratio after light activation. Box plots represent median and 25th to 75th percentiles. Whiskers show minimum and maximum points. **(D)** Relative N/C ratio over time during 488 nm activation

277 amongst optoYAP mutants.©) Absolute intensity values of mCherry signal in nuclei over time.
278 Solid lines represent mean, n=10 cells taken from three independent experiments.
279
280 We then looked at canoncial YAP regulatory sites, such as serine 127 and the C-terminal PDZ-
281 binding motif. We observed that the S127A mutant (referred to as optoYAP S127A) is nuclear
282 localised even before light activation, contrasting significantly with the wild-type cells (Fig.
283 5A-B). After light activation, we observed that optoYAP S127A accumulated further within
284 the nucleus, doubling the nuclear to cytoplasmic ratio of optoYAP S127A as compared to the
285 dark state (Fig. 5D). This shows that the optoYAP S127A mutant can exert its predominantly
286 nuclear state but optogenetic activation can intensify this ability and increase optoYAP levels
287 in the nucleus.
288
289 Deletion of the PDZ-binding motif on YAP causes complete YAP exclusion from the
290 nucleus.(32) We synthesised a truncated optoYAP without the PDZ-binding motif, which we
291 refer to as optoYAP ΔC. We observed nuclear exclusion of optoYAP ΔC before exposure to
292 light activation (Fig. 5C). Pulsatile light activation can induce nuclear localisation of optoYAP
293 ΔC, nearly doubling the amount of nuclear localised optoYAP ΔC. The optoYAP ΔC construct
294 returns to the cytoplasm after 20 minutes of recovery in the dark, similar to the wildtype and
295 S127A mutant. Therefore, activation of the optogenetic tool can overcome mutations that drive
296 YAP out of the nucleus.

297

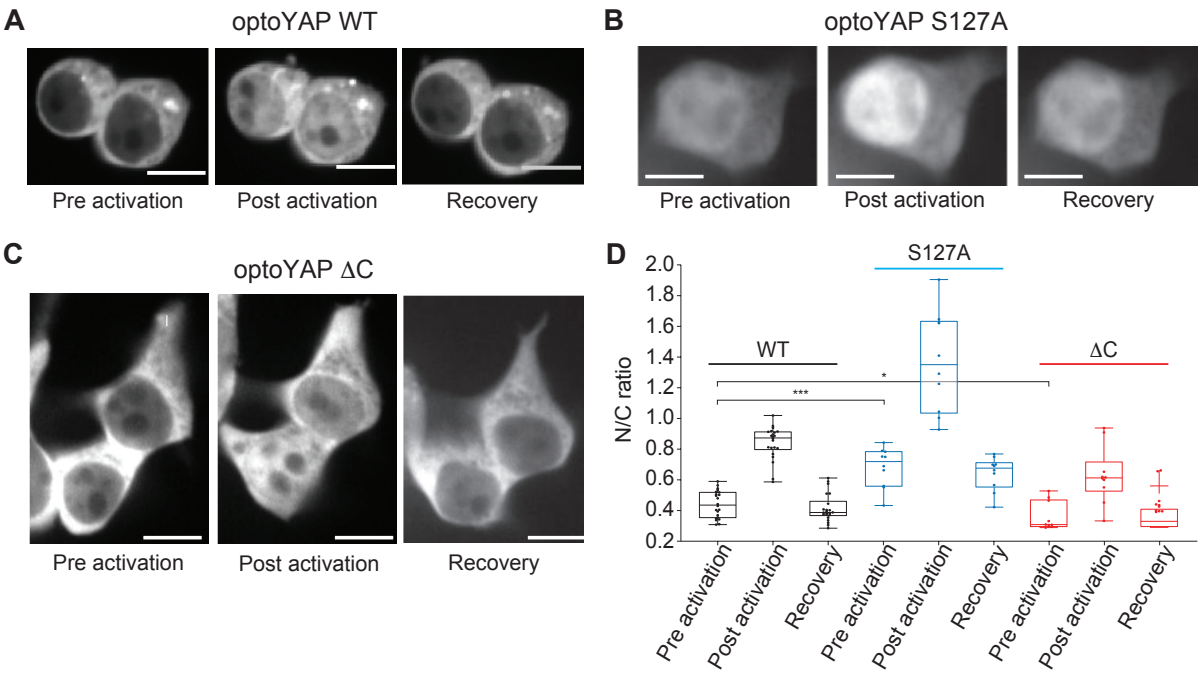

298

299 **Figure 5. optoYAP variants under light activation protocol.** Representative images of
300 mCherry signal in HEK293T cells containing **(A)** wildtype (WT) optoYAP, **(B)** optoYAP with
301 a point mutation at S127A, or **(C)** truncated optoYAP without the C-terminal PDZ-binding
302 motif (optoYAP ΔC). The 'Pre activation' panels show cells before exposure to 488 nm light,
303 and after 20 min of pulsatile activation with 488 nm light, the same cells were imaged as 'Post
304 activation'. Cells were left in the dark for a 20 min and imaged again, under the 'Recovery'
305 panel. **(D)** Quantification of nuclear to cytoplasmic ratio of optoYAP in (A-C). Box plots
306 represent median and 25th to 75th percentiles. Whiskers show minimum and maximum points.
307 Scale bars, 10 µm. n=22 cells for (A), n=10 cells for (B) and (C), taken from three independent
308 experiments. *$P < 0.05$, ***$P < 10^{-3}$.

309

310

311

312

313 **Discussion**

314

315 Here, we report that optoYAP can accelerate wound healing by promoting cell proliferation
316 and migration in different cell culture systems. We show that activation of YAP can increase
317 the rate of wound repair by 20% in cardiomyocytes. optoYAP, in the absence of endogenous
318 YAP in MKN28 cells, promotes wound healing, accelerating the time taken for closure (Fig.
319 3A). However, we observed smaller differences in the H9c2 cells between the wildtype and the
320 optoYAP transfected cells (Fig. 2A-B). We further explored the mechanisms that determine
321 the YAP nuclear-cytoplasmic localisation. We demonstrate that the defects in YAP nucleus
322 localisation by perturbation to the S127A residue and C-terminal PDZ-binding motif can be
323 compensated for through use of optoYAP activation. Taken together, our results provide strong
324 evidence that: (i) YAP can play an active role in repair beyond simply proliferation; and (ii)
325 optoYAP can regulate YAP activity, even in the presence of different perturbations to YAP,
326 which may be important for wound repair in a range of cell types.

327

328 By counting the number of cell proliferation events during wound closure, we observed a few
329 differences between the MKN28 and H9c2 cell lines. We saw that optoYAP increases the
330 amount of cell proliferation in serum starved MKN28 *YAP*$^{-/-}$ cells, but not to the wild-type
331 levels (Fig. 3B). However, in MKN28 *YAP*$^{-/-}$ cells, the lack of endogenous *YAP* reduces the
332 amount of proliferation in these cells. Despite transfection with optoYAP, the levels of YAP
333 present in MKN28 *YAP*$^{-/-}$ cells might not be the same as endogenous YAP in wild type cells.
334 Therefore, this might explain the differences between the amount of proliferation in the
335 MKN28 variants. On the contrary in H9c2 cells, activated optoYAP does not alter the amount
336 of proliferation in transfected cells (Fig. 2C). This suggests that serum starvation effectively
337 reduces cell proliferation globally. Overall, both cell lines with transfected optoYAP kept in

338 the dark had comparable numbers of proliferation to their light activated counterparts. This
339 shows that despite having similar cell proliferation, light activated optoYAP speeds up the time
340 required for wound closure in both cell lines by enhancing cell migration.
341
342 Multiple signalling pathways regulate YAP independently of Hippo, including the epidermal
343 growth factor receptor (EGFR) signalling pathway.(47) Downstream of EGFR lie the
344 Ras/Raf/MEK/ERK transduction axis, where ERK is the final kinase activator that regulates
345 transcription factors. ERK is a key regulator of regeneration and interplay between ERK and
346 YAP has been shown to be drive YAP activation. By synthesising phosphomimetics of the
347 ERK phosphorylation sites, we observed some nuclear localisation of optoYAP without light
348 activation. Nuclear localisation of YAP phosphorylated at both serine residues have been
349 observed, though a single phosphorylation mark at either S251 or S333 is sufficient to induce
350 nuclear translocation.(48,49) However, the double mutant is significantly more nuclear
351 localised than the single mutants (Fig. 4B), which shows the additive effect of phosphorylating
352 both serine residues. Despite the differences observed amongst the three optoYAP mutants, it
353 appears that mutating optoYAP at the two ERBB2 activating phosphorylation sites does not
354 significantly increase nuclear localisation of the optoYAP construct as compared to the
355 wildtype variant.
356
357 Additionally, we looked at canonical YAP regulatory sites, S127 and the PDZ-binding motif,
358 that changes the cellular distribution of YAP. Despite all three mutants having an increase in
359 nuclear localisation after light activation, it is evident that the basal level of nuclear localisation
360 is not equal. The optoYAP S127A mutant (0.68 ± 0.13) has a significantly higher initial nuclear
361 concentration than wild type (0.44 ± 0.09), since the S127A mutation causes optoYAP to be
362 predominantly nuclear. Conversely, the optoYAP ΔC mutant (0.36 ± 0.09) has a significantly

363 lower nuclear localisation compared to wild type (0.44 ± 0.09), which is expected as deletion
364 of the PDZ-binding motif prevents optoYAP from translocating into the nucleus.(32) Although
365 the basal levels differ for the three variants, nuclear localisation doubles for all optoYAP
366 variants and decreases back to their respective basal levels after recovery in the dark (Fig. 5D).
367 This shows that the optogenetic domains can promote further nuclear translocation despite
368 mutations that already boosts (S127A) or inhibit (ΔC) nuclear localisation.
369
370 The rate of nuclear localisation of the two S127A and ΔC optoYAP mutants have yet to be
371 studied, which could shed light on the dynamics of nuclear shuttling in the optoYAP mutants.
372 The rate of nuclear import or export might differ drastically between the optoYAP variants,
373 depending on the mutation. We hypothesise that the activating S127A mutation increases the
374 rate of nuclear import but does not affect nuclear export rates, while the negative ΔC mutant
375 increases the rate of nuclear export but maintains similar import rates as WT. Regardless, it is
376 evident that mutations in the S127 or PDZ-binding motif changes the initial localisation of
377 optoYAP, but the activated optogenetic construct can supersede the basal distribution and
378 induce optoYAP nuclear localisation, nonetheless.
379
380 Finally, we note that several optogenetic YAP constructs have been published recently, with
381 different YAP isoforms and activation protocols. Illes *et al.* first published a tool to control the
382 subcellular localisation of YAP by tagging it with an optogenetic NLS, shuttling YAP between
383 the cytoplasm and the nucleus.(50) The authors used the human YAP1 gene without specifying
384 the details of the splice isoform, and demonstrated that activated YAP increases proliferation
385 in 2D and 3D cultures, and induces invasion in cancer spheroids.(50) Dowbaj *et al.* presented
386 optogenetic YAP1, using the human YAP1-2γ isoform,(51) which contains exon 6 and two
387 WW domains,(52) tethering optogenetic YAP and TAZ to the mitochondria. Their tool allows

388 the study of protein dynamics by describing the rate of nuclear entry and exit, but does not
389 demonstrate downstream functionality of nuclear YAP.(51) In our previous work, we reported
390 a human YAP1-1δ optogenetic tool that translocates between the cytoplasm and nucleus,
391 demonstrating functional outputs *in vitro* and *in vivo*.(40) Most recently, Meyer *et al.* have
392 developed a mouse YAP1 tool. They are able to regulate the levels of pluripotency factors Oct4
393 and Nanog, and hence control the renewal of a naïve stem cell state or preferential
394 differentiation into the mesendodermal state.(53) The various YAP isoforms signal differently,
395 where those without exon 6, alpha and beta, can form heterodimers with TAZ.(54) Additionally,
396 different isoforms have unique and common functions and activate distinct downstream
397 transcriptional programmes.(55) Taken together, the isoforms of YAP matter when describing
398 optogenetic constructs, given that each isoform can have unique downstream effects.
399
400 The role of YAP in wound healing has been investigated previously, where nuclear localisation
401 of YAP is observed during healing.(56,57) We demonstrate that optoYAP can accelerate
402 wound healing as compared to endogenous YAP, providing a tight spatiotemporal control over
403 its activity. It has been shown that H9c2 cells respond to substrate stiffness and topography,
404 promoting cell differentiation on a modified ECM synthesized from fibroblast-derived
405 matrix.(58) With our optogenetic tool, it will be interesting to investigate cell migration in an
406 environment that mimics physiological conditions by seeding cells on permissive extracellular
407 matrix, or a stiffened matrix that imitates cholesterol plaques, and tracking wound healing
408 under such conditions, which will benefit future studies on regeneration.
409
410
411
412

413 **Materials and Methods**

414

415 Plasmid construction

416 Optogenetic plasmid containing YAP (optoYAP) was previously described by Toh et al.,
417 2022.(40) Mutant YAP containing S127A or ΔC modifications were PCR amplified from
418 pBABE (hygro) hYAP1-1δ S127A and pBABE (hygro) hYAP1-1δ ΔC plasmids respectively,
419 both of which were from the library of YAP cDNA constructs of the Sudol laboratory. These
420 constructs are available from 'Addgene' vector resource. Phusion High Fidelity DNA
421 polymerase (ThermoScientific) was used for PCR amplification with primer sequences for
422 each amplification listed in Table 1. PCR products and optoYAP plasmid were cleaved with
423 appropriate FastDigest restriction enzymes (ThermoScientific) for cloning.

424

425 Point mutations in hYAP1-1δ were generated with Q5 Site-Directed Mutagenesis Kit (NEB)
426 according to the manufacturer's instructions to synthesise phosphomimic mutants by
427 substituting serine with aspartic acid at two residues, S251 and S333. Positive clones were
428 verified by restriction enzyme digestion and sequencing. Primers used for site-directed
429 mutagenesis (SDM) are listed in Table 1.

430

431 Mammalian cell culture and transfection

432

433 HEK293T human embryonic kidney cells were grown in DMEM (ThermoScientific)
434 supplemented with 10% (v/v) heat inactivated fetal bovine serum (FBS, Gibco) and 1% (v/v)
435 penicillin/streptomycin (Gibco). MKN28 human gastric adenocarcinoma cells were grown in
436 RPMI (ThermoScientific) supplemented with 10% (v/v) FBS and 1% (v/v)
437 penicillin/streptomycin. H9c2 rat cardiomyocytes (a gift from Dr Manvendra K. Singh's lab)

438 were grown in DMEM supplemented with 15% (v/v) FBS, 1% (v/v) penicillin/streptomycin
439 and 1% non-essential amino acids (NEAA, Gibco). All cell cultures were kept in a 37ºC
440 incubator with 5% CO_2 and passaged every 2-3 days. Cells were routinely checked for
441 mycoplasma contamination and STR profiled (1st Base).
442
443 HEK293T cells were transfected with plasmid DNA using Lipofectamine 2000
444 (ThermoScientific) using 6 µL of Lipofectamine 2000 reagent in 150 µL opti-MEM
445 (ThermoScientific) and 3.5 µg of plasmid DNA in 175 µL opti-MEM according to the
446 manufacturer's instructions. H9c2 cells were transfected with Lipofectamine 2000 as per
447 HEK293T cells, but with 5 µg of plasmid DNA. MKN28 cells were transfected using K2
448 transfection system (Biontex).
449
450 Fluorescence microscopy
451
452 Live imaging was performed on Perkin Elmer spinning disk with a LUCPlanFLN 40x/0.6
453 numerical aperture (NA) air objective or Nikon Ti-E with Yokogawa W1 spinning disk with a
454 PLAN APO VC 60x/1.20 NA water immersion objective. Cells were visualised under the
455 microscope 24 h post transfection in a 37ºC heated and humidified chamber.
456
457 Long term imaging of wound healing experiments was performed on widefield Nikon
458 Biostation IMQ with 10x air objective or Olympus IX81 with a UPLFLN 10x/0.3 NA air
459 objective. The samples were tracked every 30 min to measure the rate of wound closure until
460 the gap was completely closed.
461
462 Image analysis

463

464 The images were analysed with Fiji ImageJ software. The nuclear to cytoplasmic ratio was
465 measured by drawing a region of interest (ROI) around the cell as well as its nucleus. A macro
466 plugin written by Richard De Mets was used to mask the nucleus from the cytoplasm to
467 calculate the mean intensity in the nucleus and cytoplasm based on the ROI drawn. The ROI
468 was drawn for each cell analysed at every time frame. The wound healing analysis was
469 performed using a macro written by Ong Hui Ting, which measures the changes in gap area of
470 the wound over time. Charts were made with Prism 8 software. All figures were assembled
471 with Adobe Illustrator.

472

473 Light activation

474

475 Pulsed light activation followed a protocol of 1 s pulse of 0.15 mW 488 nm laser light followed
476 by a 30 s dark phase. This pulsation is continued for 20 min, which constitutes as 'light
477 activation'. During recovery, the entire set up is kept in the dark for a further 20 min.
478 Throughout the entire 40 min of light activation and recovery, imaging was done with a 561
479 nm laser line to image the mCherry fluorescent protein. For samples kept under dark conditions,
480 aluminium foil was used to wrap the sample to prevent light contamination.

481

482 RT-qPCR

483

484 Transfected cells were subjected to 48 h of pulsatile light activation and total RNA was
485 extracted from cells using RNeasy Plus Mini Kit (QIAGEN) and QIAshredder (QIAGEN)
486 according to the manufacturer's instructions. RNA was eluted with 40 μL nuclease free water
487 (NFW) and quantitated using NanoDrop 2000 spectrophotometer. Complementary DNA

488 (cDNA) was synthesised using SuperScript IV Reverse Transcriptase (ThermoScientific) using
489 oligo d(T) primers according to the manufacturer's instructions.
490
491 Real-time PCR detection were done using SYBR Green PCR Master Mix for 40 cycles in a
492 Bio-Rad CFX96 thermal cycler. The threshold cycle (Ct) value for each gene was normalised
493 to the Ct value of a housekeeping gene, *EIF1B*. The relative fold changes were calculated using
494 ΔΔCt method. The primer sequences for target genes are listed in Table 2.
495
496 Wound healing assay
497
498 Cells were grown in their respective serum free media for 24 h before 25 000 cells per chamber
499 were plated into Culture-Insert 2 well in μ-Dish 35 mm, high (ibidi). Cells were kept in serum
500 free media throughout the experiment. 24 h after seeding, or when cells reach confluency in
501 the chambers, the culture insert was removed with clean forceps under sterile conditions and
502 the dish was filled with 2 mL of serum free media for imaging.
503
504 Anchorage-independent assay
505
506 Anchorage-independent assay was performed using CytoSelect 96-Well Cell Transformation
507 Assay (Cell Biolabs) according to the manufacturer's instructions. Cells were grown in T25
508 flasks to 80% confluency, trypsinised and counted with a hemocytometer to obtain the
509 concentration of live cells. Each well was seeded with 5000 cells and the final cell culture agar
510 layer solution was 0.4% for soft conditions and 1.2% for stiff conditions, corresponding to a
511 Young's modulus of <2 kPa(59) and 10 kPa(60) respectively. Fresh medium was changed
512 every 2 days during incubation and 7 days after seeding, cell colony formation was examined

513 with EVOS Cell Imaging System (ThermoScientific) under 10X magnification. The total
514 amount of DNA present in each well was measured with a DNA binding fluorescent dye using
515 the CyQuant NF Cell Proliferation Assay Kit according to the manufacturer's instructions.
516
517 Statistical analysis
518
519 Biological replicates refer to independent experimental replicates done on different days with
520 fresh biological samples and independent transfections and measurements. Technical replicates
521 refer to repeated measurements of the same sample that represent independent measures of the
522 random noise associated with protocols or equipment.(61) For comparisons between the same
523 sample in different light and dark conditions, a paired t-test was used. For comparisons between
524 two distinct samples, an unpaired t-test was used. For small sample sizes, estimation statistics
525 was used to show the magnitude of the testing condition.(62)
526
527 Curve fitting
528
529 Curve fitting for the import and export rates was performed in MATLAB using the curve fitting
530 function *fit*. Time constant (τ) represents the time scale over which the signal changes before
531 or after light activation. Nuclear import rate (τ_a) was fitted with $f(x) = a + b\left(1 - e^{-\frac{x}{\tau}}\right)$ and
532 export rate (τ_r) was fitted with $f(x) = a + b\left(e^{-\frac{x}{\tau}}\right)$, where a is the basal level of signal
533 intensity; and b is the multiplicative factor representing the change in signal due to light
534 (de-)activation.
535
536
537

538 **Supplementary Data**

539

Primer name	Sequence	Cloning	Restriction enzyme
PT25 hYAP1-1delta fwd	ATTTATGGTACC ATGGATCCCGGGCAG	Forward primer for S127A and ΔC mutants	KpnI
PT26 hYAP1-1delta S127A rev	CGCGCCGTTTAAACC TATAACCATGTAAG	Reverse primer for S127A	PmeI
PT27 hYAP1-1delta DeltaC rev	CGCGCCGTTTAAACC TAGCTTTCTTTATCTAGC	Reverse primer for ΔC	PmeI
795-2194-YAP-S251D-F1	GATCCACAGGGAGG CGTCATGGGTG	Forward primer for SDM of S251D mutant	-
796-2194-YAP-S251D-R1	CTGGGGAGCCAGGG GTGGTGGCTGT	Reverse primer for SDM of S251D mutant	-
797-2195-YAP-S333D-F1	GATCCCGGGATGTC TCAGGAATTGAG	Forward primer for SDM of S333D mutant	-
798-2195-YAP-S333D-R1	CGACACTGGATTTT GAGTCCCACCATC	Reverse primer for SDM of S333D mutant	-
799-2196-YAP-2mut-F1	CAGCCACCACCCCTGGC TCCCCAGGATCCACAGG GAGGCGTCATGGGTG	Forward primer for SDM of S251D and S333D mutant	-
800-2196-YAP-2mut-R1	CTCAATTCCTGAGACATC CCGGGATCCGACACTGG ATTTTGAGTCCCACCATC	Reverse primer for SDM of S251D and S333D mutant	-

540 **Table 1. List of primers for plasmid cloning.**

541

Target gene	Forward primer	Reverse primer
EIF1B	TGATGCAACT AAGGGTGACG	CAGTGTCTTT CTGCCGTTCC
CTGF	TGCATCCGTA CTCCCAAAAT	ATGTCTTCAT GCTGGTGCAG
CYR61	TCCCTGTTTT TGGAATGGAG	GAGCACTGGG ACCATGAAGT
TGF-β	TACCTGAACCC GTGTTGCTCTC	GTTGCTGAGGT ATCGCCAGGAA

542 **Table 2. Primers used for RT-qPCR.**

543

544 **Declarations**

545 Ethics approval and consent to participate

546 Not applicable

547 Consent for publication

548 Not applicable

549 Availability of data and materials

550 The datasets used and/or analysed during this study are available from the corresponding author

551 on reasonable request.

552 Competing interests

553 The authors declare that they have no competing interests.

554 Funding

555 This work was primarily supported by a Singapore Ministry of Education Tier 3 grant

556 (MOE2016-T3-1-250 002). M.S. was also supported by grants from the National University of

557 Singapore (R-185-000-2710- 133 & 733) and the Mechanobiology Institute (R-714-018-006-
558 271). T.E.S. was further supported by an EMBO Global Investigator award and startup funds
559 from University of Warwick, UK.

560 Authors' contributions

561 PJYT, MS and TES conceived the study and design of the work. PJYT performed the
562 experiments. PJYT and TES did the data analysis. PJYT and TES drafted the work with all
563 authors approving the final manuscript.

564 Acknowledgements

565 We thank Michael Sheetz, in whose lab the work on developing the optogenetic YAP construct
566 was initiated, and Manvendra Singh for comments on the manuscript.

567

568 **References**

569 1. Murry CE, Reinecke H, Pabon LM. Regeneration gaps: observations on stem cells and
570 cardiac repair. J Am Coll Cardiol. 2006 May;47(9):1777–85.

571 2. Sedmera D, Reckova M, DeAlmeida A, Coppen SR, Kubalak SW, Gourdie RG, et al.
572 Spatiotemporal pattern of commitment to slowed proliferation in the embryonic mouse
573 heart indicates progressive differentiation of the cardiac conduction system. Anat Rec
574 A Discov Mol Cell Evol Biol. 2003 Sep;274(1):773–7.

575 3. Steinhauser ML, Lee RT. Regeneration of the heart. EMBO Mol Med. 2011 Dec
576 1;3(12):701–12.

577 4. Porrello ER, Mahmoud AI, Simpson E, Hill JA, Richardson JA, Olson EN, et al.
578 Transient Regenerative Potential of the Neonatal Mouse Heart. Science (1979).
579 2011;331(6020):1078–80.

580 5. Poss KD, Wilson LG, Keating MT. Heart Regeneration in Zebrafish. Science (1979).
581 2002 Dec 13;298(5601):2188–90.

582 6. Chong JJH, Yang X, Don CW, Minami E, Liu YW, Weyers JJ, et al. Human embryonic-
583 stem-cell-derived cardiomyocytes regenerate non-human primate hearts. Nature. 2014
584 Jun;510(7504):273–7.
585 7. Liu YW, Chen B, Yang X, Fugate JA, Kalucki FA, Futakuchi-Tsuchida A, et al. Human
586 embryonic stem cell-derived cardiomyocytes restore function in infarcted hearts of non-
587 human primates. Nat Biotechnol. 2018 Aug;36(7):597–605.
588 8. Xin M, Kim Y, Sutherland LB, Murakami M, Qi X, McAnally J, et al. Hippo pathway
589 effector Yap promotes cardiac regeneration. Proceedings of the National Academy of
590 Sciences. 2013 Aug 20;110(34):13839–44.
591 9. Heallen T, Morikawa Y, Leach J, Tao G, Willerson JT, Johnson RL, et al. Hippo
592 signaling impedes adult heart regeneration. Development. 2013 Dec;140(23):4683–90.
593 10. Leach JP, Heallen T, Zhang M, Rahmani M, Morikawa Y, Hill MC, et al. Hippo pathway
594 deficiency reverses systolic heart failure after infarction. Nature. 2017
595 Oct;550(7675):260–4.
596 11. Panciera T, Azzolin L, Cordenonsi M, Piccolo S. Mechanobiology of YAP and TAZ in
597 physiology and disease. Nat Rev Mol Cell Biol. 2017;18(12):758–70.
598 12. Fu V, Plouffe SW, Guan KL. The Hippo pathway in organ development, homeostasis,
599 and regeneration. Curr Opin Cell Biol. 2017;49:99–107.
600 13. Basu S, Totty NF, Irwin MS, Sudol M, Downward J. Akt phosphorylates the Yes-
601 Associated Protein, YAP, to induce interaction with 14-3-3 and attenuation of p73-
602 mediated apoptosis. Mol Cell. 2003;11(1):11–23.
603 14. Kanai F, Marignani PA, Sarbassova D, Yagi R, Hall RA, Donowitz M, et al. TAZ: a
604 novel transcriptional co-activator regulated by interactions with 14-3-3 and PDZ domain
605 proteins. EMBO J. 2000 Dec 15;19(24):6778–91.

606 15. Zhao B, Li L, Tumaneng K, Wang CY, Guan KL. A coordinated phosphorylation by
607 Lats and CK1 regulates YAP stability through SCFβ-TRCP. Genes Dev. 2010;24(1):72–
608 85.
609 16. Vassilev A, Kaneko KJ, Shu H, Zhao Y, DePamphilis ML. TEAD/TEF transcription
610 factors utilize the activation domain of YAP65, a Src/Yes-associated protein localized
611 in the cytoplasm. Genes Dev. 2001 May 15;15(10):1229–41.
612 17. Zhang H, Liu CY, Zha ZY, Zhao B, Yao J, Zhao S, et al. TEAD Transcription Factors
613 Mediate the Function of TAZ in Cell Growth and Epithelial-Mesenchymal Transition.
614 Journal of Biological Chemistry [Internet]. 2009 May 15;284(20):13355–62. Available
615 from: https://doi.org/10.1074/jbc.M900843200
616 18. Zhao B, Ye X, Yu J, Li L, Li W, Li S, et al. TEAD mediates YAP-dependent gene
617 induction and growth control. Genes Dev. 2008;22(14):1962–71.
618 19. Yu FX, Zhao B, Guan KL. Hippo Pathway in Organ Size Control, Tissue Homeostasis,
619 and Cancer. Cell. 2015;163(4):811–28.
620 20. Moya IM, Halder G. Hippo–YAP/TAZ signalling in organ regeneration and
621 regenerative medicine. Nat Rev Mol Cell Biol. 2019;20:211–26.
622 21. Lai JKH, Toh PJY, Cognart HA, Chouhan G, Saunders TE. DNA-damage induced cell
623 death in yap1;wwtr1 mutant epidermal basal cells. Elife. 2022 May 1;11.
624 22. Wen X, Jiao L, Tan H. MAPK/ERK Pathway as a Central Regulator in Vertebrate Organ
625 Regeneration. Int J Mol Sci. 2022;23(3).
626 23. De Simone A, Evanitsky MN, Hayden L, Cox BD, Wang J, Tornini VA, et al. Control
627 of osteoblast regeneration by a train of Erk activity waves. Nature. 2021
628 Feb;590(7844):129–33.

629 24. Bassat E, Mutlak YE, Genzelinakh A, Shadrin IY, Baruch Umansky K, Yifa O, et al.
630 The extracellular matrix protein agrin promotes heart regeneration in mice. Nature.
631 2017;547(7662):179–84.
632 25. Aharonov A, Shakked A, Umansky KB, Savidor A, Genzelinakh A, Kain D, et al.
633 ERBB2 drives YAP activation and EMT-like processes during cardiac regeneration. Nat
634 Cell Biol. 2020;22(11):1346–56.
635 26. Oka T, Mazack V, Sudol M. Mst2 and Lats kinases regulate apoptotic function of Yes
636 kinase-associated protein (YAP). Journal of Biological Chemistry.
637 2008;283(41):27534–46.
638 27. Ege N, Dowbaj AM, Jiang M, Howell M, Hooper S, Foster C, et al. Quantitative
639 Analysis Reveals that Actin and Src-Family Kinases Regulate Nuclear YAP1 and Its
640 Export. Cell Syst. 2018/06/18. 2018 Jun 27;6(6):692-708.e13.
641 28. Zhao B, Wei X, Li W, Udan RS, Yang Q, Kim J, et al. Inactivation of YAP oncoprotein
642 by the Hippo pathway is involved in cell contact inhibition and tissue growth control.
643 Genes Dev. 2007;21:2747–61.
644 29. Zhang H, Pasolli HA, Fuchs E. Yes-associated protein (YAP) transcriptional coactivator
645 functions in balancing growth and differentiation in skin. Proceedings of the National
646 Academy of Sciences. 2011;108(6):2270–5.
647 30. Lamar JM, Stern P, Liu H, Schindler JW, Jiang ZG, Hynes RO. The Hippo pathway
648 target, YAP, promotes metastasis through its TEAD-interaction domain. Proc Natl
649 Acad Sci U S A. 2012 Sep;109(37):E2441-50.
650 31. Oka T, Remue E, Meerschaert K, Vanloo B, Boucherie C, Gfeller D, et al. Functional
651 complexes between YAP2 and ZO-2 are PDZ domain-dependent, and regulate YAP2
652 nuclear localization and signalling. Biochemical Journal. 2010;432(3):461–78.

653 32. Oka T, Sudol M. Nuclear localization and pro-apoptotic signaling of YAP2 require
654 intact PDZ-binding motif. Genes to Cells. 2009;14(5):607–15.
655 33. Mason DE, Collins JM, Dawahare JH, Nguyen TD, Lin Y, Voytik-Harbin SL, et al.
656 YAP and TAZ limit cytoskeletal and focal adhesion maturation to enable persistent cell
657 motility. Journal of Cell Biology. 2019 Feb 8;218(4):1369–89.
658 34. D'Angelo E, Lindoso RS, Sensi F, Pucciarelli S, Bussolati B, Agostini M, et al. Intrinsic
659 and Extrinsic Modulators of the Epithelial to Mesenchymal Transition: Driving the Fate
660 of Tumor Microenvironment. Vol. 10, Frontiers in Oncology. Frontiers Media S.A.;
661 2020.
662 35. Morikawa Y, Zhang M, Heallen T, Leach J, Tao G, Xiao Y, et al. Actin cytoskeletal
663 remodeling with protrusion formation is essential for heart regeneration in Hippo-
664 deficient mice. Sci Signal. 2015 May;8(375):ra41.
665 36. Mia MM, Cibi DM, Ghani SABA, Singh A, Tee N, Sivakumar V, et al. Loss of Yap/Taz
666 in cardiac fibroblasts attenuates adverse remodelling and improves cardiac function.
667 Cardiovasc Res [Internet]. 2022 May 15;118(7):1785–804. Available from:
668 https://doi.org/10.1093/cvr/cvab205
669 37. Zhou J. An emerging role for Hippo-YAP signaling in cardiovascular development. J
670 Biomed Res. 2014 Jul;28(4):251–4.
671 38. Fenno L, Yizhar O, Deisseroth K. The development and application of optogenetics.
672 Annu Rev Neurosci [Internet]. 2011;34:389–412. Available from:
673 https://pubmed.ncbi.nlm.nih.gov/21692661
674 39. Krueger D, Izquierdo E, Viswanathan R, Hartmann J, Pallares Cartes C, de Renzis S.
675 Principles and applications of optogenetics in developmental biology. Development
676 [Internet]. 2019 Oct 22;146(20):dev175067. Available from:
677 https://doi.org/10.1242/dev.175067

678 40. Toh PJY, Lai JKH, Hermann A, Destaing O, Sheetz MP, Sudol M, et al. Optogenetic
679 control of YAP cellular localisation and function. EMBO Rep [Internet]. 2022 Sep
680 5;23(9):e54401. Available from: https://doi.org/10.15252/embr.202154401
681 41. Liu Z, Yi L, Du M, Gong G, Zhu Y. Overexpression of TGF-β enhances the migration
682 and invasive ability of ectopic endometrial cells via ERK/MAPK signaling pathway.
683 Exp Ther Med. 2019;17(6):4457–64.
684 42. Szeto SG, Narimatsu M, Lu M, He X, Sidiqi AM, Tolosa MF, et al. YAP/TAZ are
685 mechanoregulators of TGF-b-smad signaling and renal fibrogenesis. Journal of the
686 American Society of Nephrology. 2016;27(10):3117–28.
687 43. Qin Z, Xia W, Fisher GJ, Voorhees JJ, Quan T. YAP/TAZ regulates TGF-β/Smad3
688 signaling by induction of Smad7 via AP-1 in human skin dermal fibroblasts. Cell
689 Communication and Signaling. 2018;16(1):18.
690 44. Sorensen DW, van Berlo JH. The Role of TGF-β Signaling in Cardiomyocyte
691 Proliferation. Curr Heart Fail Rep. 2020 Oct;17(5):225–33.
692 45. Peng Y, Wang W, Fang Y, Hu H, Chang N, Pang M, et al. Inhibition of TGF-β/Smad3
693 Signaling Disrupts Cardiomyocyte Cell Cycle Progression and Epithelial–Mesenchymal
694 Transition-Like Response During Ventricle Regeneration. Front Cell Dev Biol. 2021;9.
695 46. Qiao Y, Chen J, Lim YB, Finch-Edmondson ML, Seshachalam VP, Qin L, et al. YAP
696 regulates actin dynamics through ARHGAP29 and promotes metastasis. Cell Rep
697 [Internet]. 2017;19(8):1495–502. Available from:
698 http://www.sciencedirect.com/science/article/pii/S2211124717306046
699 47. Reddy BVVG, Irvine KD. Regulation of Hippo Signaling by EGFR-MAPK Signaling
700 through Ajuba Family Proteins. Dev Cell. 2013;24(5):459–71.

701 48. Bui DA, Lee W, White AE, Harper JW, Schackmann RCJ, Overholtzer M, et al.
702 Cytokinesis involves a nontranscriptional function of the Hippo pathway effector YAP.
703 Sci Signal. 2016 Mar 1;9(417):ra23–ra23.
704 49. Yang S, Zhang L, Liu M, Chong R, Ding SJ, Chen Y, et al. CDK1 Phosphorylation of
705 YAP Promotes Mitotic Defects and Cell Motility and Is Essential for Neoplastic
706 Transformation. Cancer Res. 2013 Nov 14;73(22):6722–33.
707 50. Illes B, Fuchs A, Gegenfurtner F, Ploetz E, Zahler S, Vollmar AM, et al. Spatio-selective
708 activation of nuclear translocation of YAP with light directs invasion of cancer cell
709 spheroids. iScience [Internet]. 2021;24(3):102185. Available from:
710 https://www.sciencedirect.com/science/article/pii/S258900422100153X
711 51. Dowbaj AM, Jenkins RP, Williamson D, Heddleston JM, Ciccarelli A, Fallesen T, et al.
712 An optogenetic method for interrogating YAP1 and TAZ nuclear–cytoplasmic shuttling.
713 J Cell Sci [Internet]. 2021 Jul 9;134(13):jcs253484. Available from:
714 https://doi.org/10.1242/jcs.253484
715 52. Gaffney CJ, Oka T, Mazack V, Hilman D, Gat U, Muramatsu T, et al. Identification,
716 basic characterization and evolutionary analysis of differentially spliced mRNA
717 isoforms of human YAP1 gene. Gene. 2012 Nov;509(2):215–22.
718 53. Meyer K, Lammers NC, Bugaj LJ, Garcia HG, Weiner OD. Decoding of YAP levels
719 and dynamics by pluripotency factors. Available from:
720 https://doi.org/10.1101/2022.10.17.512504
721 54. Ben C, Wu X, Takahashi-Kanemitsu A, Knight CT, Hayashi T, Hatakeyama M.
722 Alternative splicing reverses the cell-intrinsic and cell-extrinsic pro-oncogenic
723 potentials of YAP1. Journal of Biological Chemistry [Internet]. 2020;295(41):13965–
724 80. Available from:
725 https://www.sciencedirect.com/science/article/pii/S0021925817497961

726 55. Vrbský J, Vinarský V, Perestrelo AR, de La Cruz JO, Martino F, Pompeiano A, et al.
727 Evidence for discrete modes of YAP1 signaling via mRNA splice isoforms in
728 development and diseases. Genomics [Internet]. 2021;113(3):1349–65. Available from:
729 https://www.sciencedirect.com/science/article/pii/S0888754321001014
730 56. Elbediwy A, Vincent-Mistiaen ZI, Spencer-Dene B, Stone RK, Boeing S, Wculek SK,
731 et al. Integrin signalling regulates YAP and TAZ to control skin homeostasis.
732 Development. 2016 May 15;143(10):1674–87.
733 57. Lee MJ, Byun MR, Furutani-Seiki M, Hong JH, Jung HS. YAP and TAZ Regulate Skin
734 Wound Healing. Journal of Investigative Dermatology. 2014;134(2):518–25.
735 58. Suhaeri M, Subbiah R, Van SY, Du P, Kim IG, Lee K, et al. Cardiomyoblast (h9c2)
736 differentiation on tunable extracellular matrix microenvironment. Tissue Eng Part A.
737 2015 Jun;21(11–12):1940–51.
738 59. Li C, Huang Z, Wang RK. Elastic properties of soft tissue-mimicking phantoms assessed
739 by combined use of laser ultrasonics and low coherence interferometry. Opt Express.
740 2011 May;19(11):10153–63.
741 60. Nitta T, Haga H, Kawabata K, Abe K, Sambongi T. Comparing microscopic with
742 macroscopic elastic properties of polymer gel. Ultramicroscopy. 2000;82(1):223–6.
743 61. Blainey P, Krzywinski M, Altman N. Replication. Nat Methods. 2014;11(9):879–80.
744 62. Ho J, Tumkaya T, Aryal S, Choi H, Claridge-Chang A. Moving beyond P values: data
745 analysis with estimation graphics. Nat Methods. 2019;16(7):565–6.
746